

PPPL-5231

## A Predictive Model for the Tokamak Density Limit

Q. Teng, D.P. Brennan, L. Delgado-Aparicio, D.A. Gates, J. Swerdlow, R.B. White

January 2016



# Princeton Plasma Physics Laboratory

## Report Disclaimers

---

### Full Legal Disclaimer

This report was prepared as an account of work sponsored by an agency of the United States Government. Neither the United States Government nor any agency thereof, nor any of their employees, nor any of their contractors, subcontractors or their employees, makes any warranty, express or implied, or assumes any legal liability or responsibility for the accuracy, completeness, or any third party's use or the results of such use of any information, apparatus, product, or process disclosed, or represents that its use would not infringe privately owned rights. Reference herein to any specific commercial product, process, or service by trade name, trademark, manufacturer, or otherwise, does not necessarily constitute or imply its endorsement, recommendation, or favoring by the United States Government or any agency thereof or its contractors or subcontractors. The views and opinions of authors expressed herein do not necessarily state or reflect those of the United States Government or any agency thereof.

### Trademark Disclaimer

Reference herein to any specific commercial product, process, or service by trade name, trademark, manufacturer, or otherwise, does not necessarily constitute or imply its endorsement, recommendation, or favoring by the United States Government or any agency thereof or its contractors or subcontractors.

---

## PPPL Report Availability

### Princeton Plasma Physics Laboratory:

<http://www.pppl.gov/techreports.cfm>

### Office of Scientific and Technical Information (OSTI):

<http://www.osti.gov/scitech/>

---

### Related Links:

[U.S. Department of Energy](#)

[U.S. Department of Energy Office of Science](#)

[U.S. Department of Energy Office of Fusion Energy Sciences](#)

# A Predictive Model for the Tokamak Density Limit

Q. Teng, D.P. Brennan, L. Delgado-Aparicio, D.A. Gates, J. Swerdlow, R.B. White

*Princeton Plasma Physics Laboratory, Princeton University, Princeton, NJ, USA*

## Abstract

The Greenwald density limit, found in all tokamak experiments, is reproduced for the first time using a phenomenologically correct model with parameters in the range of experiments. A simple model of equilibrium evolution and local power balance inside the island has been implemented to calculate the radiation-driven thermo-resistive tearing mode growth and explain the density limit. Strong destabilization of the tearing mode due to an imbalance of local Ohmic heating and radiative cooling in the island predicts the density limit within a few percent. The density limit is found to be weakly dependent on impurity densities. Results are robust to a substantial variation in model parameters within the range of experiments.

## I Introduction

Toroidal confinement devices always observe an upper limit on the operational plasma density. The exact formulation of this limit evolved as better measurements became available [1, 2, 3, 4]. The most successful empirical scaling law of the density limit is known as the Greenwald density limit [5, 6],

$$\bar{n}_G [10^{20} \text{m}^{-3}] = \frac{I_p [\text{MA}]}{\pi a^2 [\text{m}^2]}, \quad (1)$$

where  $\bar{n}_G$  is the line-averaged plasma density,  $I_p$  is the plasma current and  $a$  is the minor radius of plasma. This limit is ubiquitous among different machines with various con-

figurations. A schematic graph showing the operational region on tokamaks is shown in Figure. 1. Detailed measurements are available in Figure 3 of Ref. [6]. As experiments ap-

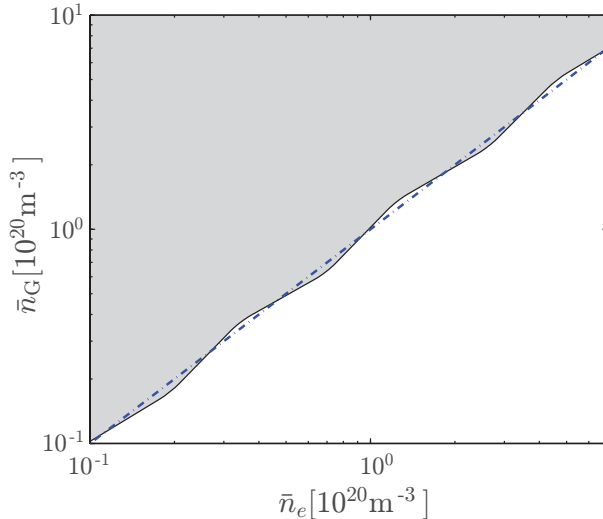


Figure 1: The blue dashed line is the the Greenwald density limit. The shaded region is the operational region of tokamaks.

proach the density limit, a series of phenomena take place including: MARFES, diverter detachment, poloidal detachment, the H-L mode transition, current channel shrinking, and finally they end by the appearance of a magnetic island usually with poloidal mode number  $m = 2$  and toroidal mode number  $n = 1$ , and a major disruption [6]. Magnetic islands are topologically isolated flux domains created by magnetic reconnection at rational surfaces [7]. An example of a 2/1 island in cylindrical geometry is shown in Fig. 2.

Many attempts have been made to explain the physics behind the density limit. Experiments show that the Greenwald density limit can be exceeded by increasing the core density, suggesting the limit to be a local limit [8]. It's also widely recognized that the density limit is associated with cooling of the edge plasma and radiation [9, 10]. In Ref. [11],

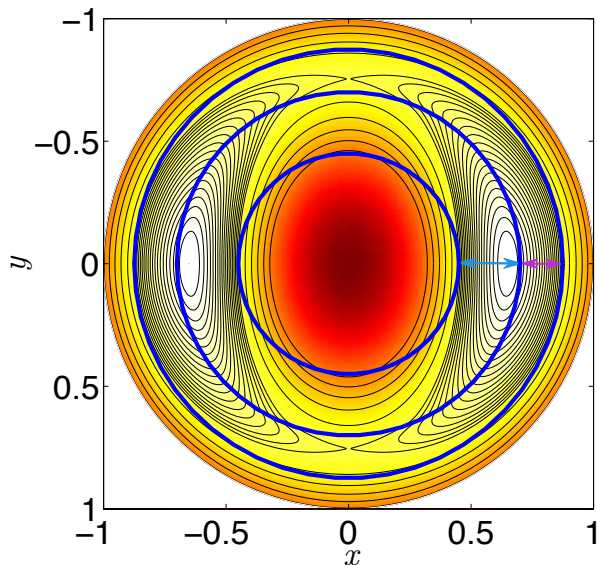


Figure 2: An example of a 2/1 island. The three blue circles are the inner edge of the island, rational surface, and outer edge of the island respectively. The brighter colors denote higher values of  $\psi$ . The asymmetry is revealed by the different lengths of the blue and purple arrows.

Rebut suggested a thermal island model to explain the limit. Cooling of the island may trigger significant growth of the island and change the topology of the magnetic configuration, leading to disruptions. This model explains the limit qualitatively. Ref. [12] extended the Rutherford equation with a radiation term and predicted exponential growth of the island, which is confirmed by experiments on Rijnhuizen Tokamak Project (RTP) in [13]. But no previous work has explained the density limit quantitatively with the correct phenomenology [14, 15].

Recently D.A. Gates *et al.* proposed a mechanism that explains the density limit using a thermo-resistive tearing mode formalism [16, 17, 18, 19]. R. B. White *et al.* completed this model by adding a crucial island asymmetry term [20]. D. P. Brennan *et al.* reproduced the exponential growth of the island, as predicted by the analytical cylindrical model, with a 3-D full MHD code DEBS [18, 21]. Scanning the low- and

high-  $Z$  impurity densities, L. Delgado-Aparicio found that the radiative power density can be significantly enhanced while still obtaining the experimental  $Z_{eff}$  values [18, 22]. Since the magnetic island is thermally isolated from the surrounding plasmas, its power balance is dominated by radiative cooling and Ohmic heating. The local power balance sets the internal temperature profile of the island. As plasma density is increased, the Ohmic heating typically decreases while the radiative cooling increases. When radiation losses dominate, the temperature drop creates a negative current perturbation inside the island. The current perturbation, coupled with the asymmetry of the island, can cause substantial growth of the island and lead to disruption. This mechanism sets an upper limit on the operational plasma density. As the island growth is sensitive to radiative cooling and the cooling is sensitive to plasma density, the density limit is a very robust phenomenon.

## II The tearing mode model

We show that the thermo-resistive tearing mode model can explain the density limit quantitatively. The scan of plasma density is from  $2 \times 10^{19} \text{ m}^{-3}$  to  $2 \times 10^{20} \text{ m}^{-3}$ , with the deviation from the density limit being a few percent. The stiffness of this model is shown by varying the parameters assumed in the model within the range of experiments. This work is focused on island growth on the  $q = 2$  surface, where  $q$  is the safety factor denoting the local field line helicity, but the model is applicable to the island at any rational surface. The island growth rate is calculated by the modified Rutherford equation (MRE) [20]

$$\frac{dw}{dt} = 1.66 \frac{\eta}{\mu_0} [\Delta'_{classic}(w) + \Delta'_{rad}(w) + \Delta'_A(w)], \quad (2)$$

where  $w$  is island width.  $\Delta'_{classic}$  is the classical term first derived in [23];  $\Delta'_{rad}$  is the current perturbation term caused by radiation;  $\Delta'_A$  is the island asymmetry term. For small island width, approximate expressions of the last two terms are derived [20],

$$\Delta'_{rad}(w) = \frac{16\mu_0\langle\delta j_1\rangle}{\psi_0''} \frac{w}{w^2 + w_F^2}, \quad \Delta'_A(w) = \frac{2\mu_0 j'(r_x)}{\pi\psi_0''} \frac{w^2}{w^2 + w_F^2} A_s f_F, \quad (3)$$

where  $\langle\delta j_1\rangle$  is the current perturbation integrated over the island interior,  $\psi_0''$  is the second derivative of zeroth order helical flux,  $w_F$  is the Fitzpatrick critical island width [24, 25],  $r_x$  is the location of the X-point,  $A_s = (r_x - r_l)/(r_r - r_x) - 1$  is the island asymmetry,  $r_l$  and  $r_r$  are the left and right edges of the island at the maximum width, and  $f_F$  is the Fitzpatrick factor accounting for the degree of current profile flattening inside the island ( $f_F$  is chosen to be 1 in our calculation). As  $\psi_0''$  and  $j'(r_x)$  are always negative,  $\Delta'_{rad}$  (for a negative  $\langle\delta j_1\rangle$ ) and  $\Delta'_A$  are both destabilizing. An example of the three  $\Delta'$  terms with  $q_0 = 0.9$ ,  $q_{edge} = 3.7$  is shown in Fig. 3. When the island width is much smaller than  $w_F$  (about  $0.01a$ ),  $\Delta'_{classic}$  dominates the island growth.  $\Delta'_{rad}$  and  $\Delta'_A$  dominate only when the island is sufficiently large. Thus our present cylindrical model requires a finite size seed island, i.e. the island being linearly unstable or due to perturbation from other sources.

The temperature profile inside the island is determined by

$$\frac{3}{2} \frac{\partial(n_e T)}{\partial t} = \nabla \cdot (\chi_{\perp} \nabla(n_e T)) + P_{\text{input}} - P_{\text{loss}}, \quad (4)$$

where  $\chi_{\perp}$  is the cross field electron thermal diffusivity inside the island. As shown in Ref. [20], in steady state, this equation can be simplified to a first order differential equation,

$$0 = \chi_{\perp} \psi_0''(r_s) n_e(r_s) \frac{dT}{d\psi} + P_{\text{input}} - P_{\text{loss}}, \quad (5)$$

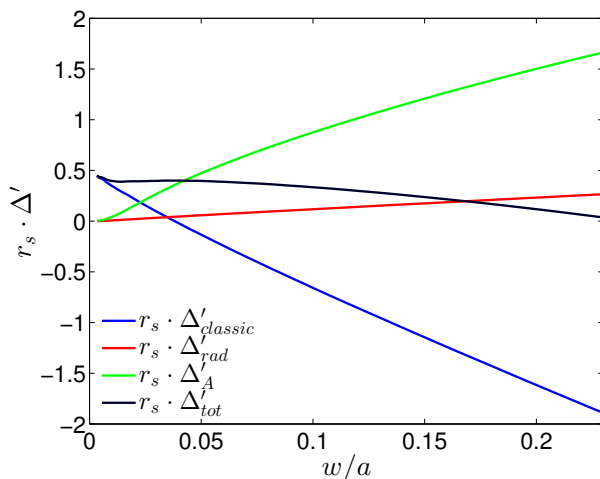


Figure 3: Characteristic  $\Delta'$  evolution with island width  $w$ .

where  $\psi$  is the helical flux. The boundary condition is set by the equilibrium temperature at the separatrix of the island.

### III Equilibrium evolution model

To associate the local power balance criterion with the global density limit, a set of cylindrical tokamak-like equilibria is assumed. The current density profile and safety factor profile are given by [26]

$$j(r) = \frac{j_0}{[1 + (r/r_0)^{2\nu}]^{1+1/\nu}}, \quad q(r) = q_0 [1 + (r/r_0)^{2\nu}]^{1/\nu}, \quad (6)$$

where  $j_0$  is the current density on the axis,  $r_0$  is the width of the current channel,  $\nu$  is a parameter controlling the peakedness of the current profile,  $q_0 = 2B_\phi/(\mu_0 R j_0)$  is the safety factor on the axis,  $B_\phi$  is the constant toroidal magnetic field, and  $R$  is the major radius. A parabolic density profile is also assumed

$$n_e(r) = n_{e0} \left( 1 - \left( \frac{r}{a} \right)^2 \right), \quad (7)$$

where  $n_{e0}$  the plasma density on the axis. In this simplified cylindrical model, the equilibrium is set by three constraints. For each equilibrium, we choose a set of  $q_0$ ,  $q_{\text{edge}}$  and line-averaged plasma density  $\bar{n}_e$ . The third parameter constraining the equilibrium,  $\nu$ , is calculated with an *ad hoc* relation between  $\bar{n}_e$  and normalized internal inductance  $l_i$ . In cylindrical geometry,  $l_i$  is defined as

$$l_i = \frac{2\pi \int_0^a B_\phi^2(r) r dr}{\pi a^2 B_\phi^2(a)} = 2 \left[ 1 + \left( \frac{a}{r_0} \right)^{2\nu} \right]^{2/\nu} \int_0^a dr \frac{r^3}{a^4 \left[ 1 + \left( \frac{r}{r_0} \right)^{2\nu} \right]^{2/\nu}}, \quad (8)$$

where  $r_0 = \left[ \left( \frac{q_{\text{edge}}}{q_0} \right)^\nu - 1 \right]^{-1/2\nu} \cdot a$ . In Ref. [10], it is found experimentally (JET) that there is an upper and a lower limit on  $l_i$ . The upper limit of  $l_i$  corresponds to the density limit that we aim to investigate in this work. The limits are fitted with [16]

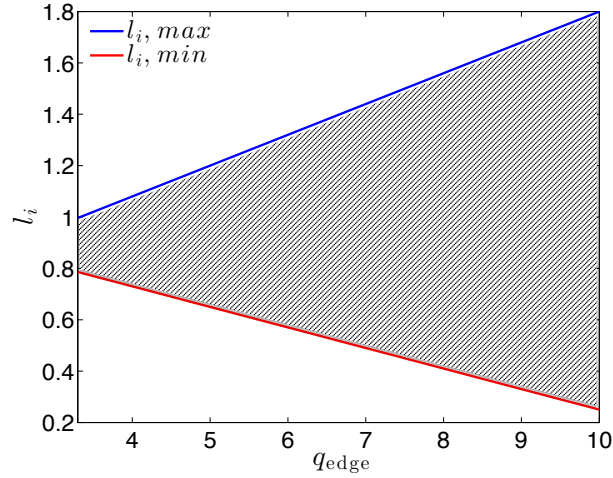


Figure 4: Schematic stability diagram for JET. The upper limit shows the density limit disruptions. The lower limit is the kink and double tearing region. The shaded region is the operational region.

$$l_{i,max} = (0.12q_{\text{edge}} \cdot h + 0.6) \cdot h, \quad l_{i,min} = (-0.08q_{\text{edge}} \cdot h + 1.05) \cdot h, \quad (9)$$

where  $q_{\text{edge}} = 2\pi a^2 B_\phi(a)/(\mu_0 R I)$  is the edge safety factor, and  $h = (1 + \kappa^2)/(2\kappa)$  approximates the modifications of  $l_i$  and  $q_{\text{edge}}$  due to elongation  $\kappa$  (here  $\kappa=1.9$ ). To mimic experiments we assume an *ad hoc* model to relate  $l_i$  and  $\bar{n}_e$ ,

$$l_i(n_e) = \begin{cases} (l_{i,\text{max}} - l_{i,\text{min}}) \frac{\bar{n}_e/\bar{n}_G - 0.7}{0.3} + l_{i,\text{min}} & \text{if } \bar{n}_e/\bar{n}_G > 0.7 \\ l_{i,\text{min}} & \text{if } \bar{n}_e/\bar{n}_G \leq 0.7 \end{cases}. \quad (10)$$

An example of the *ad hoc* relation and four alternative relations are shown in Fig. 5. Later in this work, it will be shown that the thermo-resistive tearing mode formalism is robust to the choice of this relation. With  $q_0, q_{\text{edge}}$  and  $\bar{n}_e$  chosen,  $\nu$  and thus the equilibrium can be solved from Eq. (8-10). Now consider a sequence of equilibria with increasing

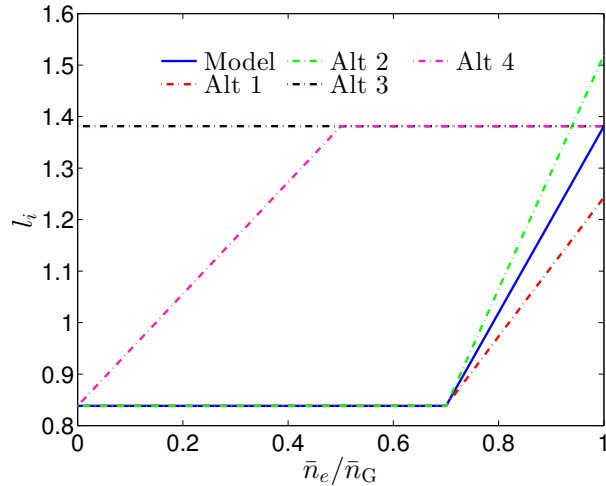


Figure 5: The *ad hoc* and alternative relations of  $l_i$  and  $n_e$ . The solid line is the  $l_i$  model given by Eq. (10). The dashed lines are four alternatives for comparison. In this case,  $q_{\text{edge}} = 3.7$ .

$\bar{n}_e$  as well as fixed  $q_0 = 0.9$  and  $q_{\text{edge}} = 3.7$ . This sequence is shown in Fig. 6, which also shows the density limit as given by  $l_{i,\text{max}}$  and the stability boundary of the tearing mode. As  $\bar{n}_e$  increases the current channel shrinks (decreasing  $r_0$ ) and becomes more peaked (increasing  $\nu$ ). The red line in Fig. 6 shows a characteristic equilibrium evolution

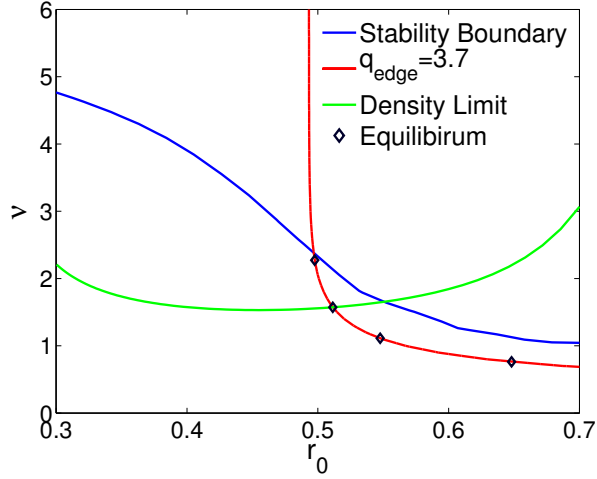


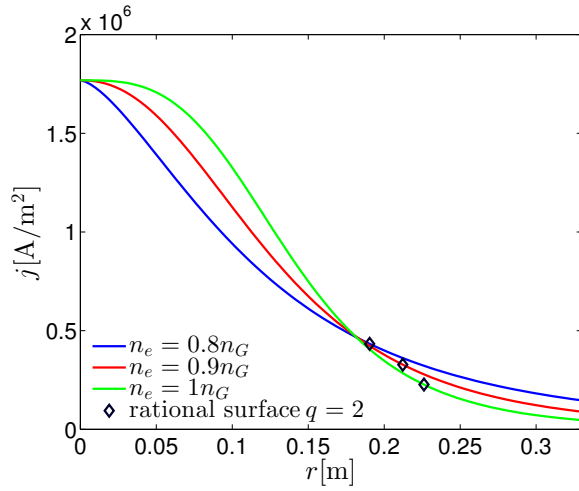
Figure 6: a) Blue: the island stability boundary under which the island is linearly unstable. b) Red: a characteristic equilibrium evolution path. c) Black diamonds: equilibria with  $\bar{n}_e/\bar{n}_G = 0.8, 0.9, 1.0, 1.1$  respectively. d) Green: the density limit.

path: when  $\bar{n}_e$  is increased towards the density limit, the island approaches the stability boundary.

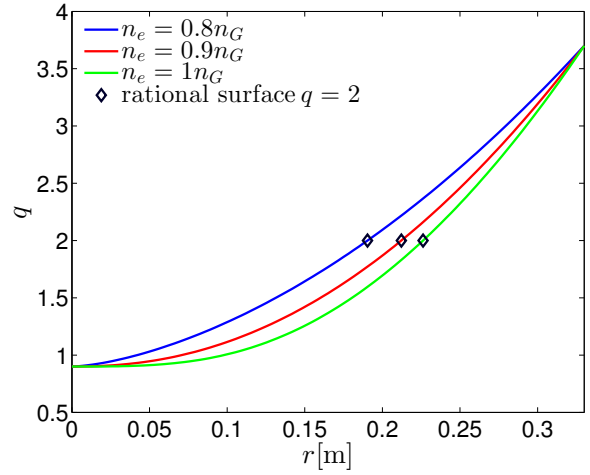
Electron resistivity is calculated by  $\eta = E/j$ . Then the Spitzer resistivity formula is used to calculate the electron temperature [27],

$$\eta = \frac{\sqrt{2m_e}Z_{\text{eff}}e^2\ln\Lambda}{12\pi^{3/2}\epsilon_0^2T_e^{3/2}} \times f(Z_{\text{eff}}), \quad f(Z_{\text{eff}}) = \frac{1 + 1.198Z_{\text{eff}} + 0.222Z_{\text{eff}}^2}{1 + 2.966Z_{\text{eff}} + 0.753Z_{\text{eff}}^2}, \quad (11)$$

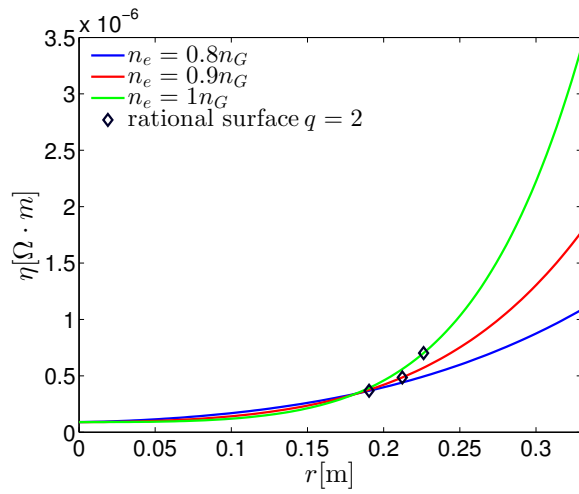
where the effective charge  $Z_{\text{eff}} = (n_D + \sum_Z n_Z \langle Z_Z \rangle^2)/n_e$  is a function of  $T_e$ ,  $\langle Z_Z \rangle$  is the average charge state of impurities,  $n_D$  and  $n_Z$  are deuterium and impurity densities respectively. An example of equilibrium profiles of  $j$ ,  $q$ ,  $\eta$  and  $T_e$  is shown in Figure. 7, using the parameters that would be explained in detail in section V, and specifically for this case choosing  $q_{\text{edge}} = 3.7$ ,  $B = 1\text{T}$ .



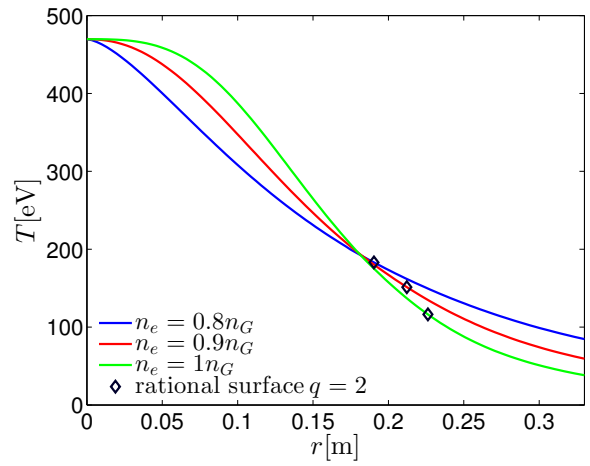
(a) current density profiles



(b)  $q$  profiles



(c) resistivity profiles



(d) temperature profiles

Figure 7: An example of equilibrium profiles with different plasma densities.

## IV Power balance inside the island

Auxiliary heat, typically deposited in the plasma center, flows along the island's separatrix and doesn't influence the power balance inside the island [24]. So the power balance inside the island is dominated by Ohmic heating and radiative cooling. The local input power density is simply given by

$$P_{\text{input}} = \eta j^2. \quad (12)$$

Plasma is cooled through Bremsstrahlung continuum radiation as well as impurity line radiation. The power loss is calculated by [22]

$$P_{\text{loss}} = n_e n_D L_D(T_e) + \sum_Z n_e n_Z L_Z(T_e), \quad (13)$$

where the cooling rate of deuterium  $L_D = 5.35 \times 10^{-37} T_e^{1/2} [\text{keV}] \text{W} \cdot \text{m}^3$ , and  $L_Z$  is the cooling rate of impurity species  $Z$ . The cooling rates of two representative impurities carbon and iron in corona equilibrium are shown in Fig. 8 [28]. In this range of temperature, iron dominates the radiation. Ref. [18] shows that a small amount of high- $Z$  impurities

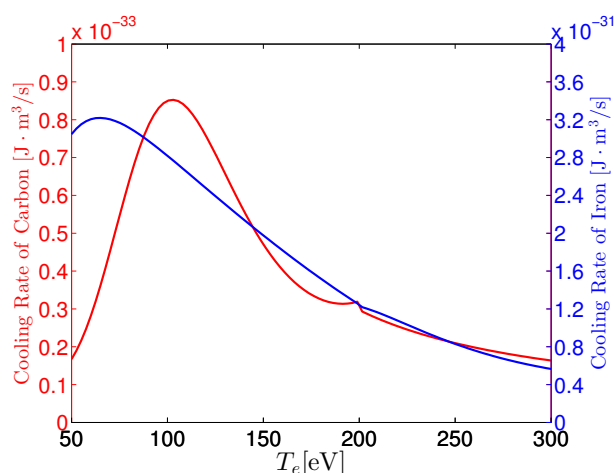


Figure 8: The cooling rate of carbon and iron. Note the cooling rate of iron is about 400 times greater than that of carbon.

can greatly increase radiation power while not changing  $Z_{\text{eff}}$  much. The density limit turns out to be a local limit, determined by power balance:  $P_{\text{rad}} < P_{\text{input}}$ , i.e. [18]

$$n_e(r_s)[10^{20}\text{m}^{-3}] < \mathcal{F}_{D,Z} \cdot j[\text{MA}/\text{m}^2] \quad (14)$$

$$\mathcal{F}_{D,Z} = \sqrt{\frac{0.61 Z_{\text{eff}} f(Z_{\text{eff}}) \cdot \ln \Lambda_{e,D}}{T_e^2[\text{keV}] \cdot \hat{P}_{\text{rad}}}} \quad (15)$$

where  $\ln \Lambda_{e,D} \approx 14.1$ ,  $\hat{P}_{\text{rad}} = P_{\text{rad}}/(n_e^2 L_D)$ . The function  $\mathcal{F}_{D,Z}$  with different impurity densities is plotted in Fig. 9.  $\mathcal{F}_{D,Z}$  is roughly constant except for when the temperature is below 100eV. This explains why the density limit is not sensitive to the temperature.

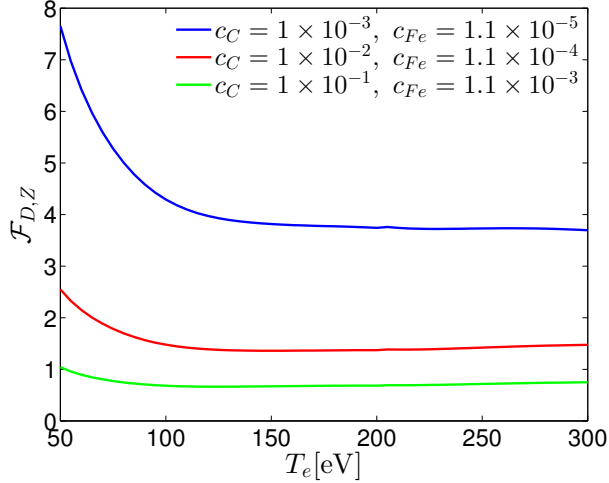


Figure 9:  $\mathcal{F}_{D,Z}$  with different impurity concentrations.  $c_Z$  is defined as  $n_Z(r_s)/n_e(r_s)$ .

A characteristic power balance inside the island with increasing  $\bar{n}_e$ , using the parameters explained in section V, and specifically for this case choosing  $q_{\text{edge}} = 3.7$ ,  $B_\phi = 3$  T and the normalized impurity densities, is shown in Fig. 10. As  $\bar{n}_e$  increases,  $j(r_s)$  decreases, hence  $P_{\text{input}}$  drops. Meanwhile,  $P_{\text{loss}}$  is proportional to  $n_e^2(r_s)$  and increases. So the net power is positive before reaching the density limit thereby suppressing the island growth. When  $\bar{n}_e$  exceeds the density limit the net power is negative thus enhancing the island growth. Fig. 11 shows that the saturated island width is very sensitive to the

plasma density when approaching the density limit. Fig. 12 shows that the temperature differential between O point and X point is small before the island grows very large.

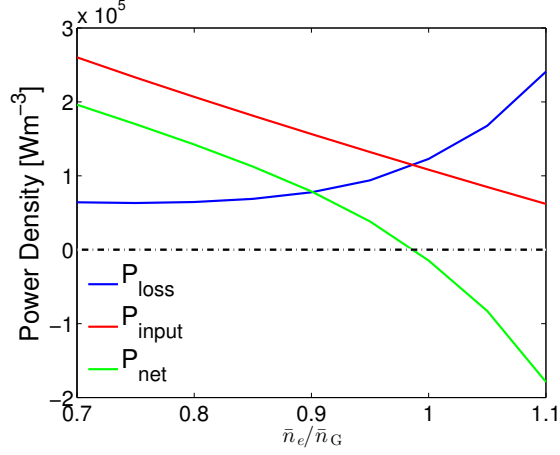


Figure 10: An example of local power balance inside the island.

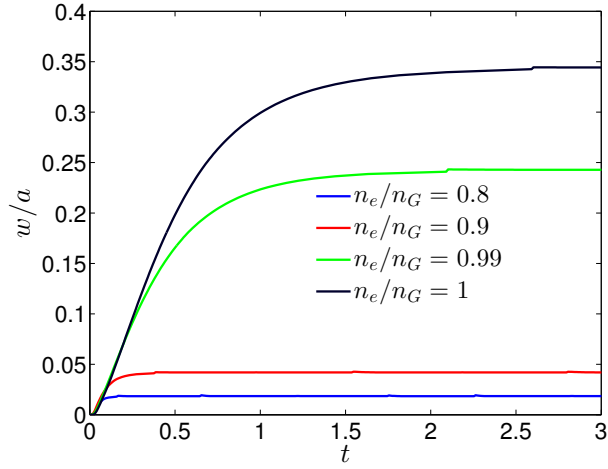


Figure 11: Island width evolution

## V Reproduce the density limit

To mimic experiments, parameters are chosen as: major radius  $R = 1$  meter,  $a = 0.33$  meter,  $q_0 = 0.9$ ,  $q_{\text{edge}}$  varied from 3.3 to 6,  $B_\phi$  varied from 1 to 4 T, constant toroidal

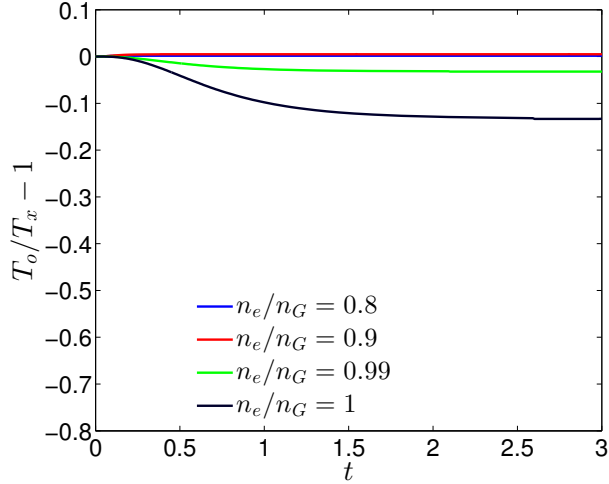


Figure 12: Temperature evolution

electric potential  $U = 1$  V, carbon density  $n_c(r_s) = 1\%n_e(r_s)$ , iron density  $n_{Fe}(r_s) = 1.1 \times 10^{-4}n_e(r_s)$  (referred to as the normalized impurity densities in this paper) and  $\chi_{\perp} = 0.13$  m<sup>2</sup>/s [29, 30]. Here iron represents the effect of all medium- to high-Z impurities; thus the density is larger than actual iron density in experiments. Impurity densities are assumed to be proportional to  $n_e(r_s)$  which may not necessarily be true. But it will be shown later in this work that the dependence of the density limit on impurities is weak. The reduction of  $\chi_{\perp}$  is due to reduced turbulent transport inside the island.

In order to predict the density limit, a criterion for disruption has to be chosen. We choose the criterion of island width growing above 20% of the minor radius. Results are insensitive to the choice of the threshold island width criterion because once island cooling occurs the island grows rapidly. A scan of the plasma density is performed using the parameters mentioned above and the result is shown in Fig. 13. Our choice of parameters covers  $\bar{n}_e$  from  $2 \times 10^{19}$  m<sup>-3</sup> to  $2 \times 10^{20}$  m<sup>-3</sup>, which includes the operational regime of most tokamaks. The local power balance criterion and island width criterion agree with the density limit within 3%. The sharp limit is determined by the strong dependence

of radiative loss on plasma density and the strong sensitivity of island growth to local power balance. This explains why the density limit is such a robust phenomenon. Every tokamak includes impurities causing radiative cooling and leading to disruption at some plasma density. The minimum irreducible amount of impurities determines the upper limit of plasma density at which a tokamak can operate.

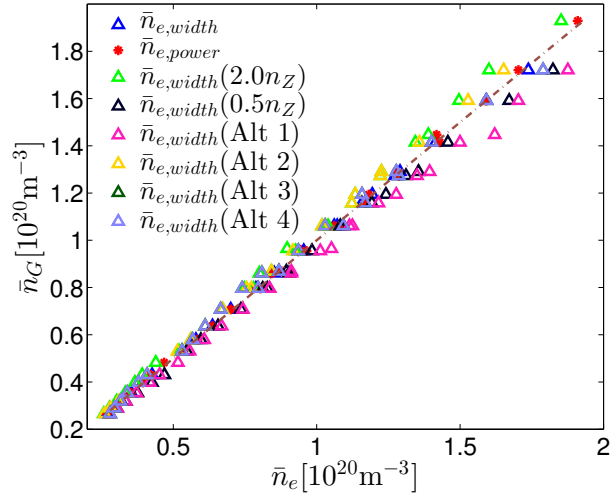


Figure 13: Variation of the density limit with varying assumptions. a) The blue triangles are the density limit from the island width criterion using the *ad hoc*  $l_i$  model normalized impurity density. b) The asterisks use the same model as a) except using the local power balance criterion. c) The light green/black triangles use 2/0.5 times the normalized impurity densities. d) The purple/yellow/green/light blue triangles use Alt 1/Alt 2/Alt 3/Alt 4  $l_i$  models.

The effect of varying the current profile peakedness on the density limit is shown in Fig. 14. In this case  $q_{edge} = 3.7$ ,  $B=1\text{T}$ . This figure shows that if  $l_i$  is kept small, the maximum achievable density can be increased by 50%. However, generally in experiments,  $l_i$  increases as  $\bar{n}_e$  is increased. Thus plasma follows the green trajectory and reaches the maximum achievable density at  $\bar{n}_G$ . The impact of impurity densities on the density limit

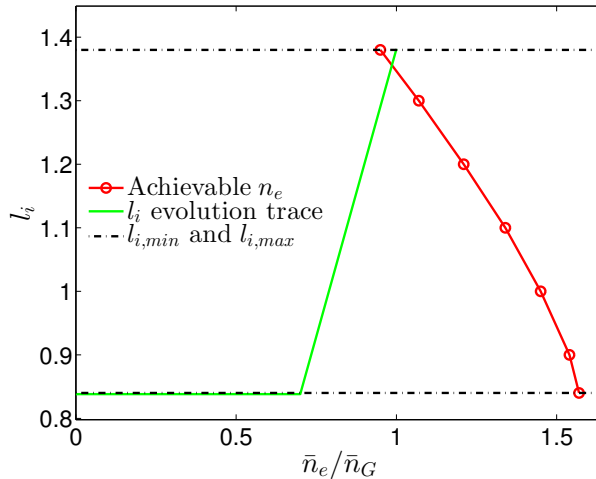


Figure 14: Density limit on the  $l_i - \bar{n}_e$  plane showing the effect of current profile variation within experimental bounds on the achievable density.

is isolated by fixing  $l_i$ , shown in Fig. 15. In this case  $q_{\text{edge}} = 4, B_\phi = 3$  T. Changing impurity densities by an order of magnitude, the density limit varies by no more than 2.5 times. This is because when impurity densities are increased,  $Z_{eff}$  increases and  $T_e$  increases as  $\eta$  is fixed. The cooling rate  $L_Z$  then decreases. This effect is canceling the impact of impurity densities on radiation power. Thus the dependence of the density limit on impurity densities is weaker than  $n_Z^{-0.5}$  as one would expect from Eq. 15. This explains why the density limit scaling law is the same for all tokamaks. It also implies that the density limit can't be improved much by reducing the impurity densities.

## VI Summary

In this work, we reproduced the Greenwald density limit quantitatively using representative experimental parameters. The thermo-resistive tearing mode model predicts the robust onset of a 2/1 tearing mode, as observed in experiments. The power balance crite-

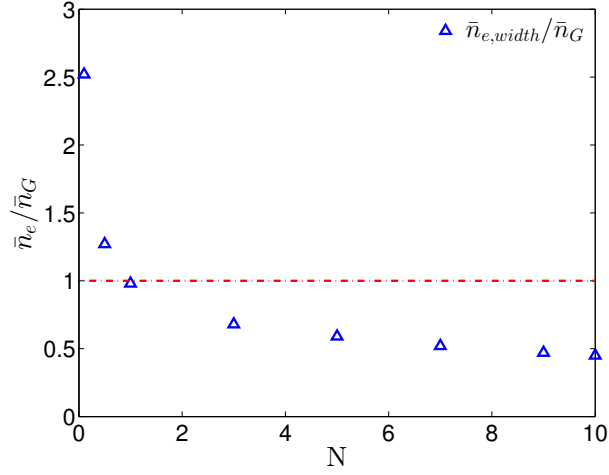


Figure 15: Impact of impurity densities on the density limit.  $N$  is the ratio of  $n_c$  and  $n_{Fe}$  over their values in the normalized impurity densities.

tion predicted by the model is an accurate criterion for the density limit. The density limit is found to be weakly dependent on the impurity densities in tokamaks. The robustness of this model is proved by its weak dependence on the parameters we used. However, this model is still simplified and limited in many aspects. Future publications will explore the effects of toroidal geometry, nonlinear mode coupling and turbulence effects on particle, heat and impurity transport. The higher order islands may grow first from radiative cooling since they are closer to the impurity sources and are in a lower temperature region of the plasma. The mechanism for rapid island growth presented in this work should be robust given any island of sufficient size, thus leading to an inward propagating collapse and disruption.

## VII acknowledgements

The first author would like to thank A. Reiman, G. Dong and Di Hu for fruitful discussions about the tearing mode theory. This work was supported by the U.S. Department of Energy Grant under Contract Nos. DE-AC02-09CH11466 and DE-SC0004125.

## References

- [1] M. Murakami, J. Callen, and L. Berry, “Some observations on maximum densities in tokamak experiments,” *Nuclear Fusion*, vol. 16, p. 347, 1976.
- [2] S. Fielding, J. Hugill, G. McCracken, J. Paul, R. Prentice, and P. Stott, “High-density discharges with gettered torus walls in dite,” *Nuclear Fusion*, vol. 17, pp. 1382–1385, 1977.
- [3] J. Hugill, P. Lomas, and A. Wootton, “High density operation in dite with neutral beam injection,” tech. rep., UKAEA Culham Lab., Abingdon, 1983.
- [4] S. Costa, R. De Angelis, S. Ortolani, and M. Puiatti, “Total radiation measurements in the eta-beta ii experiment,” *Nuclear Fusion*, vol. 22, no. 10, p. 1301, 1982.
- [5] M. Greenwald, J. Terry, S. Wolfe, S. Ejima, M. Bell, S. Kaye, and G. Neilson, “A new look at density limits in tokamaks,” *Nuclear Fusion*, vol. 28, no. 12, p. 2199, 1988.
- [6] M. Greenwald, “Density limits in toroidal plasmas,” *Plasma Physics and Controlled Fusion*, vol. 44, no. 8, p. R27, 2002.

- [7] H. P. Furth, J. Killeen, and M. N. Rosenbluth, “Finite-resistivity instabilities of a sheet pinch,” *Physics of Fluids (1958-1988)*, vol. 6, no. 4, pp. 459–484, 1963.
- [8] M. Valovic, J. Rapp, J. Cordey, R. Budny, D. McDonald, L. Garzotti, A. Kallenbach, M. Mahdavi, J. Ongena, V. Parail, *et al.*, “Long timescale density peaking in jet,” *Plasma physics and controlled fusion*, vol. 44, no. 9, p. 1911, 2002.
- [9] W. Suttrop, K. Buchl, J. Fuchs, M. Kaufmann, K. Lackner, M. Maraschek, V. Mertens, R. Neu, M. Schittenhelm, M. Sokoll, *et al.*, “Tearing mode formation and radiative edge cooling prior to density limit disruptions in asdex upgrade,” *Nuclear fusion*, vol. 37, no. 1, p. 119, 1997.
- [10] J. Wesson, R. Gill, M. Hugon, F. Schüller, J. Snipes, D. Ward, D. Bartlett, D. Campbell, P. Duperrex, A. Edwards, *et al.*, “Disruptions in jet,” *Nuclear Fusion*, vol. 29, no. 4, p. 641, 1989.
- [11] P. Rebut and M. Hugon, “Thermal instability and disruptions in a tokamak,” *Plasma Physics and Controlled Nuclear Fusion Research, London (IAEA 1985)*, vol. 2, p. 197, 1984.
- [12] P. H. Rutherford *PPPL Report-2277*, 1985.
- [13] F. Salzedas, F. Schüller, A. Oomens, R. Team, *et al.*, “Exponentially growing tearing modes in rijnhuizen tokamak project plasmas,” *Physical review letters*, vol. 88, no. 7, p. 075002, 2002.
- [14] F. Perkins and R. Hulse, “On the murakami density limit in tokamaks and reversed-field pinches,” *Physics of Fluids (1958-1988)*, vol. 28, no. 6, pp. 1837–1844, 1985.

- [15] W. M. Stacey, “Density limits in tokamaks,” *Physics of Plasmas (1994-present)*, vol. 4, no. 4, pp. 1069–1079, 1997.
- [16] D. A. Gates and L. Delgado-Aparicio, “Origin of tokamak density limit scalings,” *Physical review letters*, vol. 108, no. 16, p. 165004, 2012.
- [17] D. Gates, L. Delgado-Aparicio, and R. White, “Physics of radiation-driven islands near the tokamak density limit,” *Nuclear Fusion*, vol. 53, no. 6, p. 063008, 2013.
- [18] D. A. Gates, D. P. Brennan, L. Delgado-Aparicio, and R. B. White, “The tokamak density limit: A thermo-resistive disruption mechanism,” *Physics of Plasmas*, vol. 22, no. 6, p. 060701, 2015.
- [19] D. A. Gates, D. P. Brennan, L. Delgado-Aparicio, Q. Teng, and R. B. White, “Thermo-resistive disruptions and the tokamak density limit,” *Physics of Plasmas*, 2016. Accepted for publication in Special Issue.
- [20] R. B. White, D. A. Gates, and D. P. Brennan, “Thermal island destabilization and the greenwald limit,” *Physics of Plasmas*, vol. 22, no. 2, p. 022514, 2015.
- [21] D. P. Brennan, Q. Teng, D. A. Gates, L. Delgado-Aparicio, and R. B. White, “Simulations of radiation driven islands at the density limit,” *Physics of Plasmas*, 2016. To be submitted.
- [22] L. Delgado-Aparicio and D. A. Gates, “Onset criteria for radiation-driven tearing modes near the density limit,” *Physics of Plasmas*, 2016. To be submitted.
- [23] R. B. White, D. Monticello, M. N. Rosenbluth, and B. Waddell, “Saturation of the tearing mode,” *Physics of Fluids*, vol. 20, no. 5, pp. 800–805, 1977.

- [24] R. Fitzpatrick, “Helical temperature perturbations associated with tearing modes in tokamak plasmas,” *Physics of Plasmas*, vol. 2, no. 3, pp. 825–838, 1995.
- [25] J. Snape, K. Gibson, T. O’Gorman, N. Barratt, K. Imada, H. Wilson, G. Tallents, I. Chapman, *et al.*, “The influence of finite radial transport on the structure and evolution of  $m/n=2/1$  neoclassical tearing modes on mast,” *Plasma Physics and Controlled Fusion*, vol. 54, no. 8, p. 085001, 2012.
- [26] P. H. Rutherford, “Nonlinear growth of the tearing mode,” *Physics of Fluids*, vol. 16, no. 11, p. 1903, 1973.
- [27] A. Kuritsyn, M. Yamada, S. Gerhardt, H. Ji, R. Kulsrud, and Y. Ren, “Measurements of the parallel and transverse spitzer resistivities during collisional magnetic reconnection),” *Physics of Plasmas*, vol. 13, no. 5, p. 055703, 2006.
- [28] D. E. Post, R. Jensen, C. Tarter, W. Grasberger, and W. Lokke, “Steady-state radiative cooling rates for low-density, high-temperature plasmas,” *Atomic data and nuclear data tables*, vol. 20, no. 5, pp. 397–439, 1977.
- [29] S. Inagaki, N. Tamura, K. Ida, Y. Nagayama, K. Kawahata, S. Sudo, T. Morisaki, K. Tanaka, T. Tokuzawa, *et al.*, “Observation of reduced heat transport inside the magnetic island o point in the large helical device,” *Physical review letters*, vol. 92, no. 5, p. 055002, 2004.
- [30] K. Ida, K. Kamiya, A. Isayama, and Y. Sakamoto, “Reduction of ion thermal diffusivity inside a magnetic island in jt-60u tokamak plasma,” *Physical review letters*, vol. 109, no. 6, p. 065001, 2012.

# Princeton Plasma Physics Laboratory Office of Reports and Publications

Managed by  
Princeton University

under contract with the  
U.S. Department of Energy  
(DE-AC02-09CH11466)

---

P.O. Box 451, Princeton, NJ 08543  
Phone: 609-243-2245  
Fax: 609-243-2751

E-mail: [publications@pppl.gov](mailto:publications@pppl.gov)

Website: <http://www.pppl.gov>